

How Do Clusters in Phase-Separating Active Matter Systems Grow? A study for Vicsek activity in systems undergoing vapor-solid transition

Subhajit Paul^{1,2}, Arabinda Bera^{1,3}, and Subir K. Das^{1,3,*}

¹ *Theoretical Sciences Unit, Jawaharlal Nehru Centre for Advanced Scientific Research, Jakkur P.O, Bangalore 560064, India*

² *Institut für Theoretische Physik, Universität Leipzig, IPF 231101, 04081, Leipzig, Germany and*

³ *School of Advanced Materials, Jawaharlal Nehru Centre for Advanced Scientific Research, Jakkur P.O, Bangalore 560064, India*

(Dated: November 5, 2020)

Via molecular dynamics simulations we have studied kinetics of vapor-“solid” phase transition in an active matter model in which self-propulsion is introduced via the well-known Vicsek rule. The overall density of the particles is chosen in such a way that the evolution morphology consists of disconnected clusters that are defined as regions of high density of particles. Our focus has been on understanding the influence of the above mentioned self-propulsion on structure and growth of these clusters by comparing the results with those for the passive limit of the model that also exhibits vapor-“solid” transition. While in the passive case the growth occurs due to standard diffusive mechanism, the Vicsek activity leads to a very rapid growth, via a process that is practically equivalent to the ballistic aggregation mechanism. The emerging growth law in the latter case has been accurately estimated and explained by invoking information on velocity and structural aspects of the clusters into a relevant theory. Some of these results are also discussed with reference to a model for the active Brownian particles.

PACS numbers: 47.70.Nd, 05.70.Ln, 64.75.+g

I. INTRODUCTION

There have been much research activities in the domain concerning kinetics in systems undergoing phase transitions [1–43]. For conserved order-parameter dynamics [1–7], while significant progress has been made with respect to the understanding of structure and dynamics during phase separation in passive systems [1–5, 8–16], in the subdomain of active matter systems [17–43], though intense, the interest is rather recent. The basic questions that many of these studies ask are by concerning how the self-propulsion, a property inherent in the constituents of an active matter system, affects the universality classes [1–4] associated with such evolution dynamics. It is worth noting that there exist different types of self-propulsion. Influence of one type, on the structure and dynamics, is expected to be different from the other. Primary objective of this work is to identify the effects of a certain type of self-propulsion, that encourages the particles to align their directions of motion with each other [36], like in a system of inelastically colliding granular particles [44], on evolution during vapor-“solid” transition with a morphology that consists of well-separated clusters of “solid” phase, with short range order.

In the case of passive matter, following quenches of homogeneous configurations to state points inside the miscibility gap [1, 2], as the evolution towards the phase-separated new equilibrium occurs, the average size (ℓ) of particle-rich and particle-poor domains typ-

ically grows algebraically, with time (t), as [1–4]

$$\ell \sim t^\alpha. \quad (1)$$

The patterns, formed by the above mentioned domains, usually exhibit the simple scaling property [3]

$$C(r, t) \equiv \tilde{C}(r/\ell), \quad (2)$$

where $C(r, t)$ is a two-point equal time correlation function, defined as [3]

$$C(r, t) = \langle \psi(\vec{r}, t) \psi(\vec{0}, t) \rangle - \langle \psi(\vec{r}, t) \rangle \langle \psi(\vec{0}, t) \rangle. \quad (3)$$

In Eq. (3) ψ is a space (\vec{r}) and time dependent order parameter field, a scalar quantity for the present problem, and \tilde{C} is a time-independent master function. The scalar notation r , for the separation between two points in space, in the argument of C , is used with the understanding that there exists structural isotropy. The scaling property of Eq. (2) implies that the growth is self-similar in nature [3], i.e., apart from a change in the global length scale, the patterns at two different times are similar to each other, in a statistical sense. We repeat, in addition to this scaling property, in the passive situation, a good degree of understanding has been obtained [1–4, 45] on the analytical forms of the correlation function and values of the growth exponent α , based on the conservation of order parameter, transport mechanism, space dimension (d), overall density or composition of the system, etc.

For active matter systems there has been growing interest in recent times [17–20, 23–30, 39, 40] in the

understanding of the above mentioned aspects, viz., the scaling behavior of structure, corresponding analytical form and the growth law. There exist interest in both aligning and nonaligning dynamic (or active) interactions, e.g., in systems containing Vicsek-like [36] active particles and active Brownian particles (ABP) [35]. Given that the universality classes associated with dynamics, particularly with the evolution dynamics that is being discussed here [3], are not very robust, there exists the need for examining situations of different types. As mentioned above, already in the passive case the universality is decided by a variety of factors. In each of these cases, the influence of an activity can be different from the others, this being true for all types of self-propulsion. Our objective here is to quantify how the Vicsek [36] activity alters the class associated with the kinetics of phase separation in a system with low density of particles that gives rise to disconnected cluster morphology [13, 14, 46]. For comparative purpose we have also presented some results from an ABP system.

Many studies, with the above mentioned purpose, use models that do not exhibit phase transition in the passive limit. In such a situation, the effects of activity, in certain ways, is less transparent. Following recent works [40, 41], here we consider a model that has a passive limit which also undergoes phase transition. In these earlier works [40, 41] focus was on the understanding of pattern, growth and aging for high enough particle density so that the resulting vapor-liquid transition exhibits percolating or bicontinuous evolution morphology consisting of elongated high and low density regions of active particles. In contrast, here we undertake a comprehensive study to quantify the influence of Vicsek-like alignment activity on the kinetics of vapor-“solid” transition in $d = 2$, for disconnected morphology, that is achievable when the density of particles is rather low. We report important results on both structure and growth.

The rest of the paper is organized as follows. In Section II we discuss the model and methods. Results are presented in Section III. Finally, Section IV concludes the paper with a brief summary and outlook.

II. MODEL AND METHODS

The passive interaction among the particles, in our study, has been modeled via the potential [46–49]

$$u(r) = U(r) - U(r_c) - (r - r_c) \left(\frac{dU}{dr} \right)_{r=r_c}, \quad (4)$$

where

$$U(r) = 4\epsilon \left[\left(\frac{\sigma}{r} \right)^{12} - \left(\frac{\sigma}{r} \right)^6 \right], \quad (5)$$

the standard Lennard-Jones (LJ) pair interaction energy, with ϵ and σ being the strength and diameter of interaction, respectively. Here r is the inter-particle distance and $r_c (= 2.5\sigma)$ is a cut-off radius only within which the particles interact. The phase diagram, in the temperature (T) - density (ρ) plane, for the vapor-liquid transition that this passive model exhibits, has been estimated earlier, for $d = 2$ as well [46]. The obtained values for the critical temperature (T_c) and critical density (ρ_c) in this dimension are $\simeq 0.41\epsilon/k_B$ and $\simeq 0.37$, respectively, k_B being the Boltzmann constant and density being calculated as N/V (in appropriate dimensionless unit, see below for clarification), for N particles residing within a volume V .

We have introduced the activity in the system by following a Vicsek-like [36] rule, as previously mentioned. According to this rule, a particle tries to align its velocity along the average direction [40],

$$\vec{D}_N = \frac{\sum_j \vec{v}_j}{|\sum_j \vec{v}_j|}, \quad (6)$$

of its neighbors contained within the circle of radius r_c , with \vec{v}_j being the velocity of the j th neighbor. As explained below, this interaction is implemented in our simulations in such a way that at each instant of time the particles will get only directional impact along respective \vec{D}_N , in addition to experiencing forces due to the passive interactions.

We perform time-step driven molecular dynamics (MD) simulations [47, 48] in $2D$ square boxes of linear dimension $L\sigma$, with periodic boundary conditions applied in both the directions. The dynamical equations are numerically integrated by using the Verlet velocity algorithm [47]. To keep the temperature of the system constant, we have used the Langevin thermostat [47, 48]. Thus, for particle i , we have worked with the equation [34, 35, 40, 47] (the dots imply time derivatives)

$$m_i \ddot{\vec{r}}_i = -\nabla u_i - \gamma m \dot{\vec{r}}_i + \sqrt{(2\gamma k_B T m)} \vec{R}_i(t) + \vec{f}_i, \quad (7)$$

where m_i is the mass (same for all the particles), \vec{r}_i is the position, γ is the damping coefficient, u_i is the (passive) potential energy, \vec{R}_i is a random noise, \vec{f}_i is the active force [36, 40] and T is the temperature to which the system is quenched. The random noise \vec{R}_i is Delta-correlated over space and time, i.e., R_i^μ and R_j^ν , the μ and ν Cartesian components, corresponding to the i th and j th particles, respectively, satisfy [49]

$$\langle R_i^\mu(t) R_j^\nu(t') \rangle = \delta_{\mu\nu} \delta_{ij} \delta(t - t'), \quad (8)$$

where t and t' stand for two different times. As already stated, the force \vec{f}_i acts along \vec{D}_N , i.e.,

$$\vec{f}_i \propto f_A \vec{D}_N, \quad (9)$$

f_A being the strength of the alignment interaction [40].

Without the last term, evolution of Eq. (7), via the Verlet velocity rule, starting from time t , gives the velocity of the particles at time $t + \Delta t$ in the passive limit, where Δt is the time step of integration. In our simulations, we have used $\Delta t = 0.01\tau$, $\tau (= \sqrt{m\sigma^2/\epsilon})$ being the LJ unit of time. Following this, the particle velocities, at each time step, were further updated by incorporating \vec{f}_i . Note that Vicsek activity [36], as stated above, is supposed to change only the direction of motion. This feature is appropriately taken care of here [40]. It is known that in some active matter systems, e.g., in the case of ABP systems the temperature of the active particles settles to a value higher than the assigned number [43, 50]. Because of the nature of the active interaction in the Vicsek case [36], this possibility does not arise.

For the sake of convenience, in the rest of the paper we set m , σ , ϵ , k_B and γ to unity. All our results will be presented for $L = 1024$. The positions and velocities of all the particles, in the initial configurations, have been taken randomly, that mimics high temperature homogeneous phase. The evolution dynamics has been studied after quenching such configurations to a final temperature T below T_c , with overall density set at $\rho = 0.05$, close to the vapor branch of the coexistence curve. Final quantitative results are presented after averaging over runs with 50 independent initial configurations. Unless otherwise mentioned, all our results will be for $T = 0.1$. We have considered several values of f_A , viz., $f_A = 0, 0.5, 0.6$ and 1 , $f_A = 0$ being the passive limit. Most of the results for active case, however, are presented for $f_A = 1$. Details on the ABP model have been provided later.

For the calculation of various observables, e.g., the correlation function, we map the off-lattice configurations to lattice ones [13, 14]. Each point on the lattice has been assigned a value of ψ , the order-parameter. It is either $+1$ or -1 , depending upon whether the local density, that can be calculated from the number of particles present within a small area around that point, is higher or lower than a cut-off value ρ_{cut} . In this work, we choose $\rho_{\text{cut}} = 0.5$. Quantities like the average mass (m) of the clusters, that will turn out to be important for the quantification of growth, were calculated by appropriately identifying the boundaries of the clusters [13, 14, 51, 52].

III. RESULTS

We divide this section into two sub-sections. Results for the pure passive case are presented in the first subsection. The active matter results are presented in the second one. Unless otherwise mentioned, active

matter results will correspond to the Vicsek model.

A. Passive case

We remind the reader that our objective is to study the situation when domains of the high density phase do not percolate. So, we have chosen a low value of the overall density, viz., $\rho = 0.05$, which is significantly shifted towards the vapor branch of the coexistence curve [46], for the chosen final temperatures.

In Fig. 1(a) we show snapshots that are recorded during the evolution following the quench of a random initial configuration to $T = 0.1$. Cluster formation is quite evident even at $t = 100$, the time for the earliest snapshot. One notices that at early enough time the droplets have nearly circular appearance. With the progress of time, as the size of the droplets increases, the shape keeps deviating. The clusters at the latest presented time is very much filamental or fractal. We describe below a possible reason behind the formation of such fractal structure.

Because of the choice of a very low temperature, the clusters, i.e., the the high density regions, are in a “solid”-like state [16]. These rigid clusters are essentially static, in translational sense, and growth occurs via the diffusive deposition [5] of particles, on the larger clusters, from the vapor phase, that are supplied by the smaller clusters. Of course, during this growth process the clusters try to obtain a circular shape, requirement for the minimization of interfacial free energy, via rearrangement of the particles. However, because of the solid-like arrangement of particles [see Fig. 1(b) where we show an enlarged view of a cluster from the snapshot at $t = 2 \times 10^5$] at very low temperature, this process (with relaxation time τ_1) is not fast enough compared to the process of deposition of particles on the clusters (having relaxation time τ_2). Therefore, once the structure deviates from the circular shape, quick regaining of the shape does not become possible. Furthermore, collisions of the particles, while being deposited from the vapor phase, with the clusters, can induce random rotations in the clusters. This makes the deposition more probable in anisotropic manner, resulting in well-grown filamental structures [16].

To calculate the (mass) fractal dimension, in Fig. 2(a) we plot the average mass, m , of the clusters, as a function of the average radius of gyration, R_g . For the calculation of these quantities, as previously stated, the cluster boundaries were appropriately identified [13, 14]. Number of particles in such a closed boundary provides the mass (m_c) of the corresponding cluster. The average value was obtained from the first moment of the related distribution. The radius of gy-

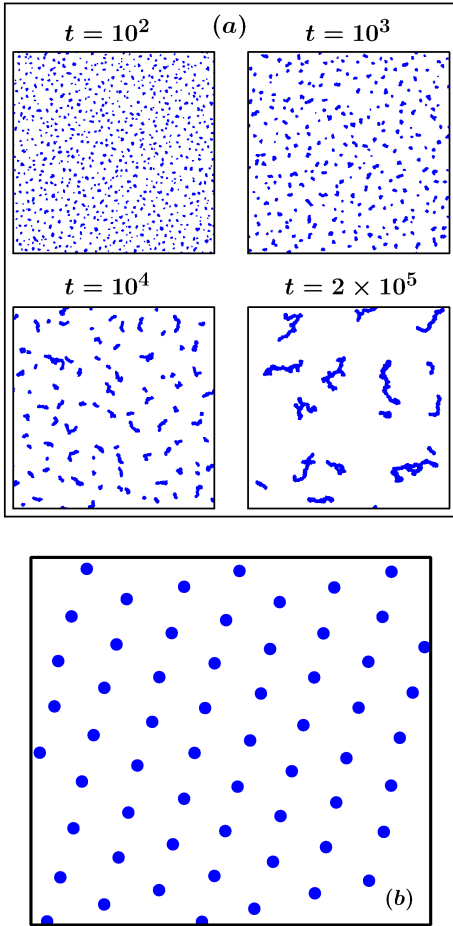


FIG. 1. (a) Snapshots during the evolution of the model, in the passive limit, are shown from four different times, following quench of a random initial configuration to $T = 0.1$. Locations of the particles are marked with dots. (b) Part of a cluster from the snapshot at $t = 2 \times 10^5$ in (a) is shown.

ration of a cluster was estimated as [53]

$$R_g^c = \left[\frac{1}{m_c} \sum_{i=1}^{m_c} (\vec{r}_i - \vec{r}_{\text{cm}})^2 \right]^{1/2}, \quad (10)$$

where \vec{r}_{cm} is the location of the centre of mass of the cluster:

$$\vec{r}_{\text{cm}} = \frac{1}{m_c} \sum_{i=1}^{m_c} \vec{r}_i. \quad (11)$$

Again, the average value was estimated from the first moment of the distribution of R_g^c . On a log-log scale, the plot in Fig. 2(a) has a linear appearance, in the large mass limit, i.e., in the long time regime. This implies a power-law behavior

$$m \sim R_g^{d_f}, \quad (12)$$

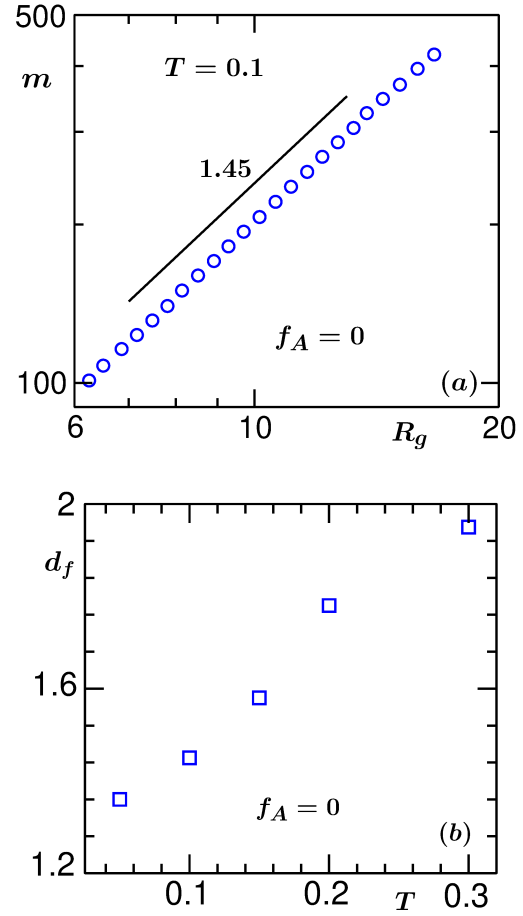


FIG. 2. (a) Average mass of clusters (m) is plotted versus the average radius of gyration (R_g), on a log-log scale, for quenches of random initial configurations to $T = 0.1$. The solid line represents a power law, exponent for which is mentioned. (b) Fractal dimension, d_f , of clusters is plotted as a function of quenched temperature. (c) Evolution snapshots are shown for two different temperatures, values of which are mentioned. In each of the cases we have chosen $t = 10^5$. All results correspond to the passive limit of the model.

d_f being the fractal dimension [54, 55]. The data set appears consistent with the solid line that has the exponent $d_f = 1.45$. Such small dimension was observed in Brownian dynamics simulations as well [56, 57], for

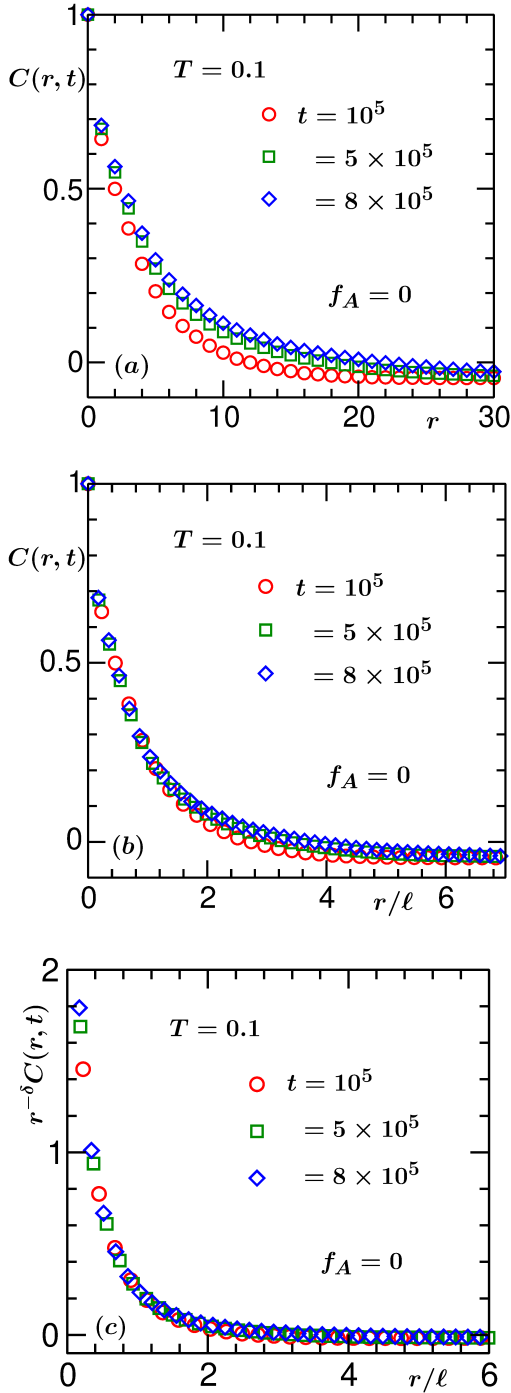


FIG. 3. (a) Two-point equal time correlation functions, $C(r, t)$, are plotted versus r , the scalar distance between two space points. Data from three different times are shown. (b) $C(r, t)$ from different times are plotted versus the scaled distance r/l . (c) Scaling plots of $C(r, t)$ are shown after taking into account the correction factor due to the fractality of the structure (see text for details). All results are from the passive limit of the model, with $T = 0.1$.

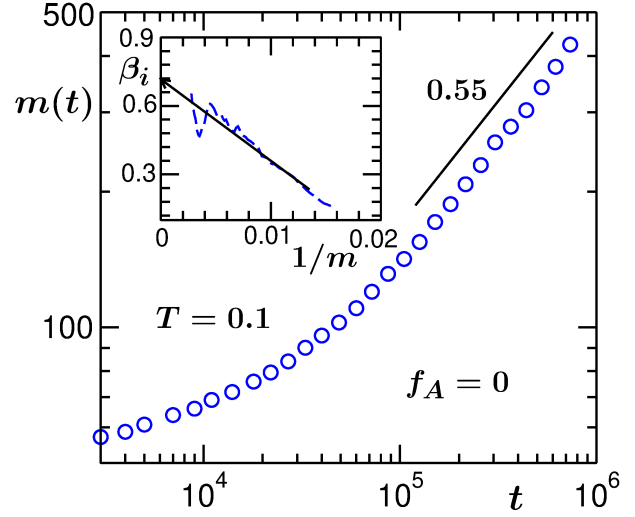


FIG. 4. Average cluster mass (m) is plotted versus time, for the passive limit of the model. The solid line represents a power-law having exponent 0.55. Inset shows β_i , the instantaneous exponent (see text for the definition), as a function of $1/m$. The arrow-headed solid line there is a guide to the eye. These results are for quenches to $T = 0.1$.

similar systems.

If the fractal structure is a result of the competition between the time scales τ_1 and τ_2 , we expect d_f to have a temperature dependence. This is because, with the increase of the latter, τ_1 decreases, whereas τ_2 increases, because of decreasing cluster rigidity and increasing density of particles in the vapor phase, respectively. In Fig. 2(b) we plot d_f as a function of T . Clearly, d_f has a strong dependence on T , the former gets enhanced with the increase of the latter. For T close to the triple point, which is around 0.3 for this model, it appears, d_f almost coincides with $d (= 2)$. For visual illustration, in Fig. 2(c) we have shown two typical snapshots, one from very low temperature and the other from $T = 0.3$. While extremely filament like structure is prominent at the lower temperature, all the clusters at $T = 0.3$ have nearly circular shape. Rest of the results are presented from $T = 0.1$, for both passive and active cases.

In Fig. 3(a) we show plots of the two-point equal time correlation function, $C(r, t)$, from different times, since the instant of quench, with the variation of distance r . Slower decay with increasing time implies growth in the system. To verify the scaling property of Eq. (2), in Fig. 3(b) we show plots of $C(r, t)$ by dividing the distance axis by the “average length” (ℓ) of the domains. The latter is obtained as the distance at which $C(r, t)$ decays to 0.25 times its maximum value that is, throughout the paper, normalized to unity. The data collapse at large values of r/l does not appear good. This is because of the fractality. In such

situations, appropriate scaling form is [54, 55]

$$C(r, t) \equiv r^\delta \tilde{C}(r/\ell), \quad (13)$$

where $\delta = d - d_f$. In Fig. 3(c) we have obtained excellent collapse of data by using the above form. The exercise in Fig. 3(c), in addition to validating the scaling form for fractal structures, confirms that our estimation of d_f is correct.

To avoid the complexity of dealing with the fractal structures, it is instructive to examine the time dependence of average mass to probe the growth in such systems. Of course, one can calculate R_g as a function of time, which is the true characteristic length. Nevertheless, we adopt time dependence of m as the marker. In Fig. 4, we have shown m as a function of t , on a log-log scale. The data at late time tend to appear linear, implying power-law growth. Here we expect

$$m \sim t^\beta, \quad \text{with } \beta = \frac{2}{3}. \quad (14)$$

This is because of the fact that the growth occurs via diffusive deposition of particles, referred to as the Lifshitz-Slyozov mechanism [5–7, 58]. However, the exponent (see the number mentioned against the solid line that is consistent with the simulation data) appears significantly lower than this expected value. This is perhaps due to the fact that nucleation is delayed and there exists an off-set length or mass when the system enters the scaling regime. In such situations, instead of extracting the exponent from the log-log plots, one should adopt more accurate exercise. In the inset of this figure we plot the instantaneous exponent [51, 52, 58]

$$\beta_i = \frac{d(\ln m)}{d(\ln t)}, \quad (15)$$

as a function of $1/m$, a standard practice in the literature for limited data span. One can appreciate that β_i , in our exercise, in the limit $m \rightarrow \infty$, converges to $\beta \simeq 0.7$, very close to the expected value.

Next we investigate how the structure and growth, observed in the passive case, get modified by the alignment interaction that is part of our general model. These findings and related explanations are provided in the next subsection. Note that the final temperature remains $T = 0.1$.

B. Active case

As stated previously, unless specifically mentioned, all results in this subsection are for Vicsek activity and with $f_A = 1$. In Fig. 5(a) we show snapshots from four different times, following quench of a homogeneous configuration, for $f_A = 1$. A comparison of

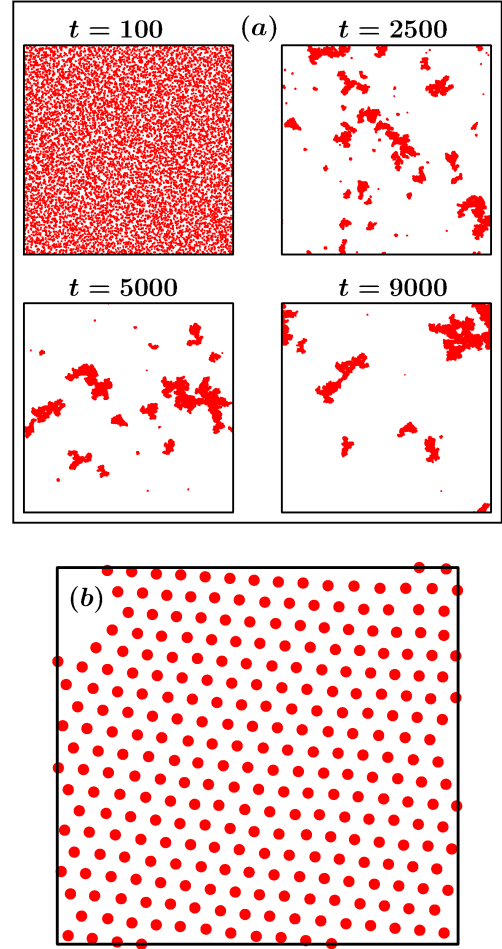


FIG. 5. (a) Evolution snapshots, following quench of a random initial configuration to $T = 0.1$, are shown from four different times, for the active case with $f_A = 1$. (b) A portion of a cluster from the snapshot at $t = 5000$ in (a) is shown. Note that the size of the portion here is larger than that in Fig. 1(b).

these snapshots with those from Fig. 1(a) reveals that the fractality is lower in this case, i.e., d_f is higher, even though the final temperature is the same. A small part of a cluster from a late time snapshot is shown in Fig. 5(b). It appears that a “solid”-like order exists even when the activity is turned on, at least for this value of f_A . As mentioned in the caption, the size of the part here is larger than that in Fig. 1(b). Because of this one may get the incorrect impression that the particle density is “much” higher inside the active clusters.

At very late time, when only a few clusters are left, there will be finite-size effects. In this limit the clusters are expected to assume circular shape, that is preferred for interfacial energy minimization, both for active and passive cases.

To estimate the fractal dimension, in Fig. 6(a) we

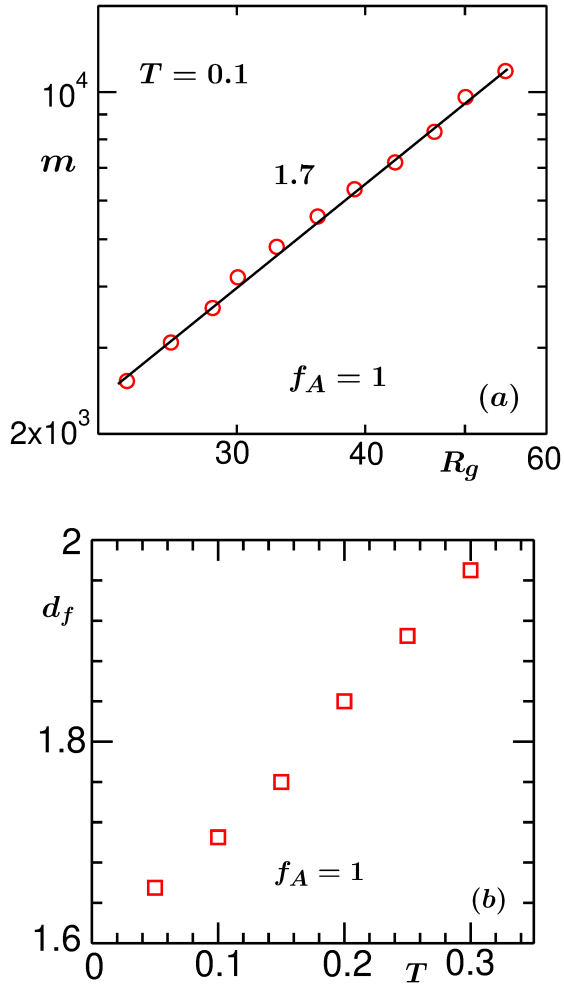


FIG. 6. (a) Log-log plot of m versus R_g , for $T = 0.1$. The solid line is a power-law, representing the fractal dimension $d_f = 1.7$. (b) Dependence of d_f on T is shown. All results are for $f_A = 1$.

have shown a log-log plot of m versus R_g , like in the previous subsection. The linear look of the data set again indicates power-law behavior and the corresponding exponent provides $d_f \simeq 1.7$. Thus the structure is indeed less fractal than the passive case. Such reduction in fractality can be due to the fact that the Vicsek [36] activity keeps the particles within the clusters, at least the ones in the peripheral regions, mobile, with respect to the centres of mass. Thus, the time scale τ_1 not being adequately smaller than τ_2 is of less relevance here. The temperature dependence of d_f , for $f_A = 1$, is presented in Fig. 6(b). Like in the passive case, here also d_f tends to d when T approaches 0.3.

In Fig. 7 we show scaling exercise for $C(r, t)$, using data from three different times. The collapse appears reasonably good when the correlation functions are plotted versus r/ℓ , even without the introduction

of r^δ . The better quality of scaling when $C(r, t)$ is plotted versus r/ℓ , compared to the passive case, is because of the higher fractal dimension, that provides a small value of δ . Next we move to quantify the growth.

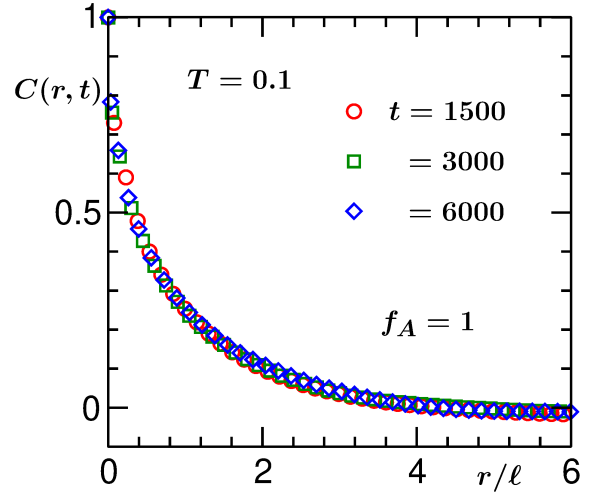


FIG. 7. $C(r, t)$, from three different times, are plotted versus r/ℓ , for the active case with $f_A = 1$ and $T = 0.1$.

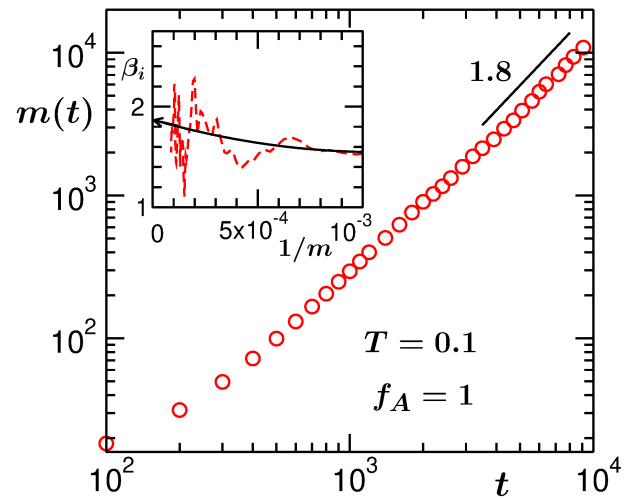


FIG. 8. For $f_A = 1$, the average mass of clusters is plotted versus time, on a log-log scale. The solid line is a power-law, exponent being mentioned next to it. Inset shows β_i as a function of $1/m$. The arrow-headed solid line there is a guide to the eye. All results are for $T = 0.1$.

Unlike the passive case, here the clusters can move, because of the activity. This may lead to growth primarily via certain cluster coalescence mechanism. For diffusive motion of the clusters, Binder and Stauffer [8–10] pointed out that the growth exponent β should be 1. This value of the exponent emerges from the

solution of the equation [10]

$$\frac{dn}{dt} = -Cn^2, \quad (16)$$

where n is the cluster density ($\propto 1/m$) and C is a constant, a consequence of the Stokes-Einstein-Sutherland relation [1, 49, 59].

In Fig. 8 we present a plot of m as a function of time, for the present problem. On the log-log scale the data set appears consistent with a power-law, at least in the long-time limit. However, the exponent is much higher than unity (see also the plot of instantaneous exponent β_i versus $1/m$, in the inset, for being better convinced), that was expected for diffusive coalescence mechanism [8–10]. A reason behind such a sharp disagreement can be the presence of fractal feature in the structure, along with a possibility that the motion of the droplets in this case is much faster than simple diffusion. To investigate the latter we calculate the mean-squared-displacement (MSD_{CM}) of the centres of mass of the clusters [49].

In Fig. 9 we show a log-log plot of MSD_{CM} , as a function of time, the latter being shifted with respect to a starting value, for a typical cluster. The data exhibit practically a quadratic behavior, implying growth due to ballistic-like aggregation mechanism [60–62], rather than the diffusive coalescence mechanism [10]. In the inset of this figure we also show the numbers of particles in a few clusters, with the progress of time. Practically flat behavior of these plots rules out the possibility of any significant contribution due to the Lifshitz-Slyozov particle diffusion mechanism.

Coming back to the plot of MSD_{CM} in the main frame of Fig. 9, as already mentioned, the time here is translated with respect to certain reference time and thus, is not related to the simulation time. One must note that such a plot here is meaningful only for the duration over which a cluster is not merging with another, following a collision. Thus the time scale of such a plot cannot match that of overall simulation.

Below we consider a theory of ballistic aggregation [30, 60–62] to see if the high value of the growth exponent, viz., $\beta \simeq 2$, can be explained. For that purpose we write the kinetic equation [16, 51, 52, 60–62]

$$\frac{dn}{dt} = - \text{“collision-cross-section”} \times v_{\text{rms}} \times n^2, \quad (17)$$

where v_{rms} is the root-mean-squared velocity of the clusters. In $d = 2$, the “collision-cross-section” is the radius of gyration which has the mass dependence $R_g \sim m^{1/d_f}$ [see Eq. (12)]. Using this, and taking $n \propto 1/m$ and $v_{\text{rms}} \sim m^{-z}$, in Eq. (17), one arrives at

$$\frac{dm}{dt} = m^{(1-zd_f)/d_f}. \quad (18)$$

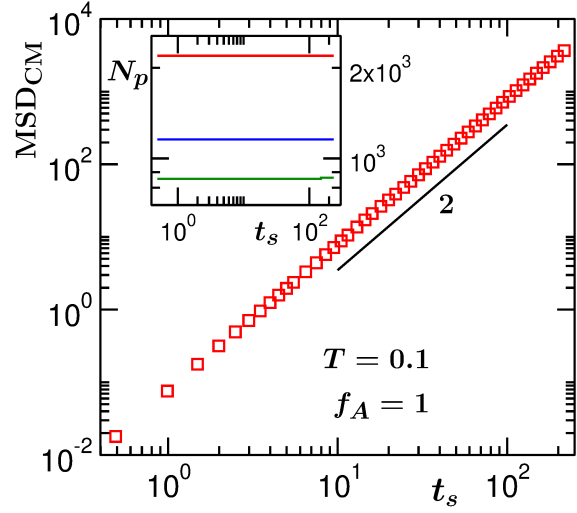


FIG. 9. Mean-squared-displacement of the centre of mass of a cluster (MSD_{CM}), for $f_A = 1$, is plotted as a function of time, on a log-log scale. The solid line is proportional to t_s^2 . The inset shows the numbers of particles (N_p) in a few different clusters, versus translated times, during periods within which they do not undergo collisions with other clusters. All results are for $T = 0.1$.

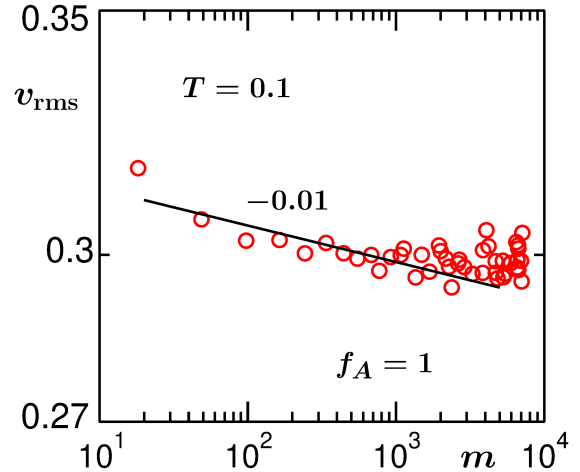


FIG. 10. Log-log plot of the root-mean-squared velocity (v_{rms}) of the clusters as a function of average mass, for $f_A = 1$ and $T = 0.1$. The solid line represents a power-law.

Solution of Eq. (18) provides [52, 62]

$$m \sim t^\beta, \quad \text{with } \beta = \frac{d_f}{d_f(z+1) - 1}. \quad (19)$$

It is worth mentioning that for such a picture to be valid, velocity relaxation, following the disturbance after a collision, should be much faster than the typical collision interval. This we have confirmed to be true via the calculations of time dependent average ve-

locity within a newly formed cluster. It appears that a constant value is rapidly reached, in fact, within a few MD steps.

Given that $d_f \simeq 1.7$ and $\beta \simeq 2$, one should have $z \simeq 0.1$, a value much smaller than 0.5, that is expected in situations when the velocities of the clusters are random, typically observed in passive matter systems [16, 52, 60–62]. In Fig. 10 we show v_{rms} as a function of m , for the present system, i.e., for $f_A = 1$. Indeed, the value appears much smaller than 0.5. The discrepancy that is observed with the expectation, i.e., $z = 0.1$, can be due to the following reason. It is possible that on an average MSD_{CM} deviates from the quadratic time dependence, to some extent. To ascertain that, of course, more accurate study, with very good statistics, is needed. However, our results are already in a very good agreement with the theoretical picture, even at a quantitative level. Here note that, since in an active matter system energy is continuously injected to each particle, from the environment, it is not surprising that v_{rms} will be nearly independent of mass.

In Fig. 11 we present growth data from a set of different non-zero values of f_A . It appears, in each of the cases the asymptotic exponent is similar. However, the onset of the latter gets delayed with the decrease of f_A . Of course, there may be minor variation in the exponent as well, e.g., due to change in d_f . More systematic study is needed to uncover this.

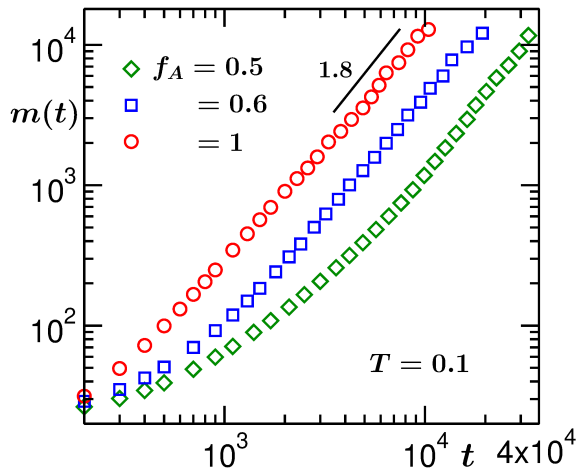


FIG. 11. Log-log plots of the average mass $m(t)$ of the clusters as a function of time, for $f_A = 0.5, 0.6$ and 1, with $T = 0.1$. The solid line represents a power-law.

To further elucidate on the role of alignment interaction in the Vicsek model, in Fig. 12 we show results for an ABP system. For this model the dynamical equations are [63]

$$\dot{\vec{r}}_i = \beta D_t [-\nabla u_i + f_p \vec{p}_i] + \sqrt{2D_t} \Lambda_i^t, \quad (20)$$

and

$$\dot{\theta}_i = \sqrt{2D_r} \Lambda_i^r. \quad (21)$$

Here \vec{r}_i is the position of the i th particle, u_i is the passive LJ potential as before, and f_p is the strength of the self-propulsion force, having direction $\vec{p}_i \equiv (\cos \theta_i, \sin \theta_i)$, whereas D_t and D_r are, respectively, the translational and rotational diffusion constants of the particles. Furthermore, in Eq. (20) and (21) Λ_i^t and Λ_i^r are the zero-mean and unit-variance Delta-correlated random noises. Note that for the passive Brownian particles $f_p = 0$. Here we have chosen $f_p = 1$. For this simulation, we have set the integration time step at $10^{-3}\tau$.

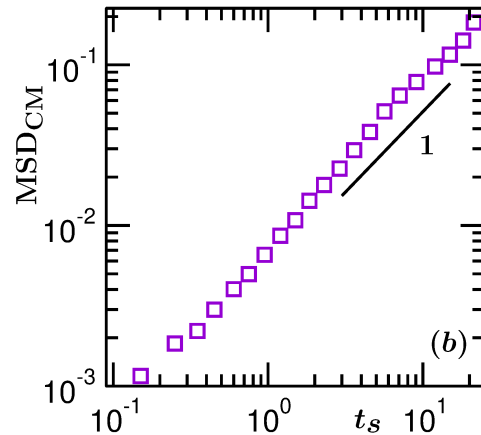
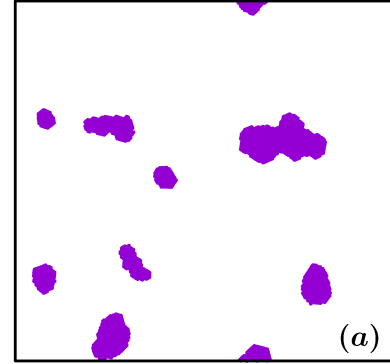


FIG. 12. (a) A typical evolution snapshot for a system containing active Brownian particles, with $f_p = 1$ and background temperature $T = 0.1$, from $t = 10^5$. (b) Depiction of time dependence of mean squared displacement of a cluster.

In part (a) of Fig. 12 we show a typical evolution snapshot. Clearly the phase separation is occurring [42]. However, the clusters in this case, as opposed to the Vicsek results, do not move ballistically. This is shown in Fig. 12(b).

IV. CONCLUSION

From extensive molecular dynamics simulations we have presented results for the kinetics of phase separation in passive and active matter systems. The passive system is the limiting case of a general active matter model. In a certain sense this set up is advantageous for the quantification of the effects of activity. The inter-particle interaction in the passive model is described by a variant of the Lennard-Jones potential [47–49]. The self-propulsion, on the other hand, for the main study on active case, is introduced via the well-known Vicsek model [36] that facilitates phase separation via cooperative motion. The overall density of particles for our studies was chosen in such a way that the morphology consisted of disconnected clusters.

In our molecular dynamics simulations, the temperature was controlled via a Langevin thermostat [47]. In the passive limit this arrangement provides growth of solid state clusters via particle diffusion mechanism [5], activated by concentration gradient. In the active case, on the other hand, we have identified that the clusters grow practically via the ballistic aggregation mechanism [16, 60–62]. Exponent for the latter appears much higher compared to the Lifshitz-Slyozov [5] value, outcome of the above mentioned diffusive mechanism. The estimated growth law for the active case we have tried to explain by incorporating the information associated with the fractality and velocity of the clusters in a relevant theory of ballistic aggregation [51, 52, 60–62]. For this purpose, identification of ballistic motion and confirmation of negligible roles of the other mechanisms were important. We have also shown that in a system of active Brownian particles such motion of clusters is non-existent.

It is expected that hydrodynamics [47, 49] will play important role in the growth process. Thus, it will be interesting to perform similar studies with a set up where active particles are immersed in a hydrodynamic solvent. Furthermore, the effects of fractality on the growth can be checked in details by varying the final temperature (T) and strength of activity (f_A). In this work we have already shown that the fractality of the solid clusters increases with the decrease of both T and f_A . Full scale studies of the kinetics with the variation of these parameters will, thus, be useful. However, such studies will bring additional complexity. The mean-squared-displacement of the clusters will have different power-law time-dependence for different combinations of T and f_A . Thus, the outcomes will be difficult to interpret. Nevertheless, this will provide a nice platform for the general understanding of cluster growth via coalescence mechanism. We intend to pursue such avenue in future. Furthermore, at a given temperature the effects of f_A may be non-monotonic [64]. To verify this one needs to consider very large range of f_A . This also we leave for a future study.

Acknowledgment: SKD acknowledges financial support from the Marie Curie Actions Plan of European Commission (FP7-PEOPLE-2013-IRSES grant No. 612707, DIONICOS); Department of Biotechnology, India (grant No. LSRET-JNC/SKD/4539); and Science and Engineering Research Board of Department of Science and Technology, India (grant No. MTR/2019/001585). SP is thankful to UGC, India, for research fellowship.

Conflicts of Interest: There are no conflicts of interest to declare.

* das@jncasr.ac.in

-
- [1] A. Onuki, *Phase Transition Dynamics*, Cambridge University Press, Cambridge, England, 2002.
 - [2] K. Binder, in *Phase Transformation of Materials*, edited by R.W. Cahn, P. Haasen, and E.J. Kramer, VCH, Weinheim, 1991, p. 405, Vol. 5.
 - [3] A.J. Bray, *Adv. Phys.*, 2002, **51**, 481.
 - [4] R.A.L. Jones, *Soft Condensed Matter*, Oxford University press, Oxford, 2008.
 - [5] I.M. Lifshitz and V.V. Slyozov, *J. Phys. Chem. Solids*, 1961, **19**, 35.
 - [6] J.G. Amar, F.E. Sullivan, and R.D. Mountain, *Phys. Rev. B*, 1988, **37**, 196.
 - [7] S. Majumder and S.K. Das, *Phys. Rev. E*, 2011, **84**, 021110.
 - [8] K. Binder and D. Stauffer, *Phys. Rev. Lett.*, 1974, **33**, 1006.
 - [9] K. Binder, *Phys. Rev. B*, 1977, **15**, 4425.
 - [10] E.D. Siggia, *Phys. Rev. A*, 1979, **20**, 595.
 - [11] H. Furukawa, *Phys. Rev. A*, 1985, **31**, 1103.
 - [12] H. Furukawa, *Phys. Rev. A*, 1987, **36**, 2288.
 - [13] S. Roy and S.K. Das, *Phys. Rev. E*, 2012, **85**, 050602.
 - [14] S. Roy and S.K. Das, *Soft Matter*, 2013, **9**, 4178.
 - [15] R. Shimizu and H. Tanaka, *Nature Comm.*, 2015, **6**, 7407.
 - [16] J. Midya and S.K. Das, *Phys. Rev. Lett.*, 2017, **118**, 165701.
 - [17] M. C. Marchetti, J. F. Joanny, S. Ramaswamy, T. B. Liverpool, J. Prost, M. Rao, and A. Simha, *Rev. Mod. Phys.*, 2013, **85**, 1143.
 - [18] S. Ramaswamy, *Annu. Rev. Cond. Mat. Phys.*, 2010, **1**, 323.
 - [19] M.E. Cates and J. Tailleur, *Annu. Rev. Cond. Mat. Phys.*, 2015, **6**, 219.
 - [20] S. Mishra and S. Ramaswamy, *Phys. Rev. Lett.*, 2006, **97**, 090602.
 - [21] J.M. Belmonte, G.L. Thomas, L.G. Brunnet, R.M.C.

- de Almeida, and H. Chaté, *Phys. Rev. Lett.*, 2008, **100**, 248702.
- [22] S. Mishra, A. Baskaran, and M.C. Marchetti, *Phys. Rev. E*, 2010, **81**, 061916.
- [23] M.E. Cates, D. Marenduzzo, I. Pagonabarraga, and J. Tailleur, *Proc. Natl. Acad. Sci. U.S.A.*, 2010, **107**, 11715.
- [24] G.S. Redner, M.F. Hagan, and A. Baskaran, *Phys. Rev. Lett.*, 2013, **110**, 055701.
- [25] G.S. Redner, A. Baskaran, and M.F. Hagan, *Phys. Rev. E*, 2013, **88**, 012305.
- [26] A. Wysocki, R.G. Winkler, and G. Gompper, *Europhys. Lett.*, 2014, **105**, 48004.
- [27] E. Méhes, E. Mones, V. Németh, and T. Vicsek, *PLOS ONE*, 2012, **7**, e31711.
- [28] F. Peruani and M. Bär, *New J. Phys.*, 2013, **15**, 065009.
- [29] S. Mishra, S. Puri, and S. Ramaswamy, *Phil. Trans. R. Soc. A*, 2014, **372**, 20130364.
- [30] P. Cremer and H. Löwen, *Phys. Rev. E*, 2014, **89**, 022307.
- [31] J. Schwarz-Linek, C. Valeriani, A. Cacciuto, M. E. Cates, D. Marenduzzo, A.N. Morozov, and W.C.K. Poon, *Proc. Natl. Acad. Sci. U.S.A.*, 2012, **109**, 4052.
- [32] J. Palacci, S. Sacanna, A.P. Steinberg, D.J. Pine, and P.M. Chaikin, *Science*, 2013, **339**, 936.
- [33] N. Kumar, H. Soni, S. Ramaswamy, and A.K. Sood, *Nature Communications*, 2014, **5**, 4688.
- [34] S.K. Das, S.A. Egorov, B. Trefz, P. Virnau, and K. Binder, *Phys. Rev. Lett.*, 2014, **112**, 198301.
- [35] B. Trefz, S.K. Das, S.A. Egorov, P. Virnau, and K. Binder, *J. Chem. Phys.*, 2016, **144**, 144902.
- [36] T. Vicsek, A. Czirók, E. Ben-Jacob, I. Cohen, and O. Schochet, *Phys. Rev. Lett.*, 1995, **75**, 1226.
- [37] A. Czirók and T. Vicsek, *Phys. A*, 2000, **281**, 17.
- [38] G. Baglietto, E.V. Albano, and J. Candia, *Interface Focus*, 2012, **2**, 708.
- [39] H. Chaté, F. Ginelli, G. Grégoire, F. Peruani, and F. Raynard, *Eur. Phys. J. B*, 2008, **64**, 451.
- [40] S.K. Das, *J. Chem. Phys.*, 2017, **146**, 044902.
- [41] S. Chakraborty and S.K. Das, *J. Chem. Phys.*, 2020, **153**, 044905.
- [42] L. Caprini, U.M.B. Marconi, and A. Puglisi, *Phys. Rev. Lett.*, 2020, **124**, 078001.
- [43] D. Loi, S. Mossa, and L.F. Cugliandolo, *Soft Matter*, 2011, **7**, 10193.
- [44] I. Goldhirsch and G. Zannetti, *Phys. Rev. Lett.*, 1993, **70**, 1619.
- [45] C. Yeung, *Phys. Rev. Lett.*, 1988, **61**, 1135.
- [46] J. Midya and S.K. Das, *J. Chem. Phys.*, 2017, **146**, 024503.
- [47] D. Frenkel and B. Smit, *Understanding Molecular Simulations: From Algorithm to Applications*, Academic Press, California, 2002.
- [48] M.P. Allen and D.J. Tildesley, *Computer Simulations of Liquids*, Clarendon, Oxford, 1987.
- [49] J.-P. Hansen and I.R. McDonald, *Theory of Simple Liquids*, Academic press, London, 2008.
- [50] D. Loi, S. Mossa, and L.F. Cugliandolo *Phys. Rev. E*, 2008, **77**, 051111.
- [51] S. Paul and S. K. Das, *Phys. Rev. E*, 2017, **96**, 012105.
- [52] S. Paul and S. K. Das, *Phys. Rev. E*, 2018, **97**, 032902.
- [53] H. Goldstein, C.P. Poole, and J.F. Saffo, *Classical Mechanics*, 3rd Ed., Addison-Wesley, 2001.
- [54] T. Vicsek, *Fractal Growth Phenomena*, World Scientific, Singapore, 1992.
- [55] T. Vicsek, M. Shlesinger, and M. Matsushita, editors, *Fractals in Natural Sciences*, World Scientific, Singapore, 1994.
- [56] F. Sciortino and P. Tartaglia, *Phys. Rev. Lett.*, 1995, **74**, 282.
- [57] F. Sciortino, A. Belloni, and P. Tartaglia, *Phys. Rev. E*, 1995, **52**, 4068.
- [58] D.A. Huse, *Phys. Rev. B*, 1996, **34**, 7845.
- [59] S. K. Das, J. V. Sengers and M. E. Fisher, *J. Chem. Phys.*, 2007, **127**, 144506.
- [60] G.F. Carnevale, Y. Pomeau, and W.R. Young, *Phys. Rev. Lett.*, 1990, **64**, 2913.
- [61] E. Trizac and P.L. Krapivsky, *Phys. Rev. Lett.*, 2003, **91**, 218302.
- [62] E. Trizac and J.-P. Hansen, *J. Stat. Phys.*, 1996, **82**, 1345.
- [63] J. Stenhammer, D. Marenduzzo, R.J. Allen, and M.E. Cates, *Soft Matter*, 2014, **10**, 1489.
- [64] E. Mani and H. Löwen, *Phys. Rev. E*, 2015, **92**, 032301.